Available online at www.sciencedirect.com
SCIENCE DIRECT®
ELSEVIER
Earth and Planetary Science Letters 211 (2003) 189–203
EPSL
www.elsevier.com/locate/epsl

Water solubility in Mg-perovskites and water storage capacity in the lower mantle☆

Konstantin Litasov[a,*], Eiji Ohtani[a], Falko Langenhorst[b], Hisayoshi Yurimoto[c], Tomoaki Kubo[a], Tadashi Kondo[a]

[a] *Institute of Mineralogy, Petrology and Economic Geology, Faculty of Science, Tohoku University, Aoba-ku, Sendai 980-8578, Japan*
[b] *Bayerisches Geoinstitut, Universität Bayreuth, 95440 Bayreuth, Germany*
[c] *Department of Earth and Planetary Sciences, Tokyo Institute of Technology, Tokyo, Japan*

Received 18 September 2002; received in revised form 15 January 2003; accepted 4 April 2003

Abstract

The water storage capacity of the major constituent of the lower mantle, Mg-perovskite, is a matter of debate. Here we report water solubility of Mg-perovskites with different compositions observed in peridotite and MORB systems. IR spectra of pure $MgSiO_3$-perovskite show bands at 3397, 3423, 3448, and 3482 cm^{-1} and suggest about 100 ppm H_2O. The H_2O content in Al-Mg-perovskite (4–7 wt% Al_2O_3; Mg# = 100) is 1000–1500 ppm (major band at 3448 cm^{-1}), whereas Al-Fe-Mg-perovskite in MORB (Al_2O_3 = 13–17 wt%; Mg# = 58–61) contains 40–110 ppm H_2O (major band at 3397 cm^{-1}). The H_2O content in Al-Fe-Mg-perovskite observed in peridotite (Al_2O_3 = 5–6 wt%; Mg# = 88–90) is 1400–1800 ppm (major band at 3397 cm^{-1}). Al-Fe-Mg-perovskite from the MORB system has a high Fe^{3+} content, $Fe^{3+}/\Sigma Fe = 0.6$, determined by electron energy loss spectroscopy measurements. Water can enter into the perovskite structure with oxygen vacancies originating from the substitution of Si by Al and Fe^{3+}. Oxygen vacancy incorporation is favored for aluminous perovskite synthesized from the MgO-rich peridotite system. The substitution of $Si^{4+}+Mg^{2+} = 2(Al,Fe)^{3+}$ prevails however in the Al-Fe-Mg-perovskite from the MORB system (MgO-poor, Al- and Fe-rich), explaining its restricted water solubility. The maximum amount of water stored in the lower mantle is estimated to be 3.42×10^{21} kg, which is 2.5 times the present ocean mass. Comparison of the phase relations in hydrous pyrolite and hydrous MORB indicates that pyrolite is more important as water container and water carrier in the mantle. Pyrolite contains: (1) dense hydrous magnesium silicates, existing under conditions of subducting slabs, and (2) hydrous wadsleyite, hydrous ringwoodite and water-bearing perovskite under the normal mantle and hotter conditions. Distribution of water to the MORB is restricted at the conditions of the transition zone and lower mantle.

Keywords: perovskite; lower mantle; water; high pressure and temperature

1. Introduction

Recent experimental and theoretical studies suggest that water plays a key role in the geodynamics of the Earth's interior because it significantly affects melting, phase transitions and physical properties of minerals. Ringwood [1]

* Corresponding author. Tel.: +81-22-2176666; Fax: +81-22-217-6675.
E-mail address: klitasov@ganko.tohoku.ac.jp (K. Litasov).

☆ Supplementary data associated with this article can be found at doi:10.1016/S0012-821X(03)00200-0

0012-821X/03/$ – see front matter
doi:10.1016/S0012-821X(03)00200-0

postulated the presence of about 2 wt% H_2O in the Earth's source material, based on the assumption that the Earth was formed from a mixture of C1 and enstatite chondrites. Although H_2O or molecular H may have been partially lost since the Earth's birth, many data suggest that a considerable amount of water can be stored in the Earth's interior. Hydrogen is also considered a possible candidate for a light element in the core [2,3]. Subduction of oceanic lithosphere into the mantle is continuously replenishing water reservoirs of the deep Earth. However, data on the water storage capacity of the different layers within the Earth is still very controversial.

Experimental data on water solubility in minerals of the Earth's mantle suggest that upper mantle, transition zone and lower mantle could have different potentials for storing water. The upper mantle is relatively dry. Water is stored in minor phases such as amphibole and phlogopite, and in low-temperature minerals related to cold subducted slabs (e.g. serpentine, chlorite, and phase A) [4–6]. Major upper mantle minerals, such as olivine, pyroxene and garnet can accommodate small amounts of water in the form of hydroxyl defects [7–10].

The transition zone should be an important water reservoir due to the significant (2–3 wt% H_2O) water solubility in $(Mg,Fe)_2SiO_4$ wadsleyite and ringwoodite [9,11,12]. Lower-temperature assemblages include water-bearing dense magnesium silicates such as phase E, Egg, phase G/D/F, and superhydrous phase B [6,12–15].

The water storage capacity of the lower mantle is a matter of debate. At lower temperatures (<1300°C), superhydrous phase B and phase G (D/F) can accommodate water in the uppermost lower mantle. The lower mantle consists of Mg-perovskite, magnesiowüstite and Ca-perovskite, however the water solubility in these minerals is poorly studied. Meade et al. [16] reported results of Fourier transform infrared (FTIR) measurements of water solubility in $MgSiO_3$-perovskite synthesized at 27 GPa and documented two pleochroic hydroxyl absorbance peaks at 3423 and 3483 cm^{-1}. Calculation of the water content yielded 60–70 ppm H_2O. However, Bolfan-Casanova et al. [17,18] showed absence of water (<1 ppm H_2O) in $MgSiO_3$-perovskite and trace amounts (<5 ppm) of H_2O in Mg-perovskite with 1–4 wt% FeO and 2–6 wt% Al_2O_3 obtained in experiments at 24 GPa. Recent data on water solubility in peridotite-related Al-Fe-Mg-perovskite measured by secondary ion mass spectrometry (SIMS) and FTIR revealed 0.1–0.4 wt% H_2O [19]. However, broadening of FTIR spectra observed in water-containing perovskites and the identification of the broad absorption bands have not been clarified.

In this paper we present water solubility in Mg-perovskites from peridotite and mid-ocean ridge basalt (MORB) systems. Using the measured water content of Mg-perovskites we estimate here the water storage capacity in the Earth's lower mantle.

2. Experimental procedures

2.1. Experiments

The phase relations were examined for pressures of 25–26 GPa and temperatures ranging from 1000 to 1600°C. We used several starting materials (Table 1) corresponding to pure $MgSiO_3$-, Al-bearing perovskite, and different perovskite compositions expected in primitive mantle (pyrolite) and MORB systems [20–22]. The hydrous compositions were prepared by adding $Mg(OH)_2$ to the synthetic mineral mixtures and adjusting the MgO proportion. A Kawai (MA8) multianvil apparatus driven by a cubic guide block and the 3000-ton press system of Tohoku University, Sendai was used in the experiments. The truncated edge length of the WC anvil was 2.0 mm. A double Pt/Re or Pt (for Fe-free samples) capsule was employed as sample container. Semi-sintered zirconia was used as pressure medium; a cylindrical $LaCrO_3$ heater was used as the heating element. Temperature was measured with a W3%Re–W25%Re thermocouple. The furnace assemblies used in the experiments are shown in Litasov and Ohtani [23].

The pressure was calibrated at 1600–2000°C by using the β–γ phase boundary of Mg_2SiO_4 [24], the decomposition boundary of ringwoodite into

Table 1
Compositions of starting materials

	Sample	SiO_2	TiO_2	Al_2O_3	FeO	MgO	H_2O
A	$MgSiO_3$+10 wt% H_2O	53.9	–	–	–	36.1	10
B	Al-MgPv (1)+10 wt% H_2O	48.4	–	9.1	–	32.5	10
C	Al-MgPv (1)	53.8	–	10.0	–	36.2	–
D	Al-MgPv (2)+5 wt% H_2O	37.3	–	12.7	–	45.0	5
E	Al-MgPv (2)+10 wt% H_2O	35.4	–	12.0	–	42.6	10
F	Al-Fe-MgPv (1)+5 wt% H_2O	33.4	1.6	14.4	26.7	18.9	5
G	Al-Fe-MgPv (2)+8 wt% H_2O	36.5	–	13.8	22.6	19.1	8
H	Al-Fe-MgPv (3)+10 wt% H_2O	47.1	–	4.6	7.2	31.1	10

Al-MgPv (1) = $MgSiO_3$+10 wt% Al_2O_3.
Al-MgPv (2) = MORB-related Al-perovskite, where FeO is replaced by MgO.
Al-Fe-MgPv (1) = MORB-related Al-Fe-Mg-perovskite [22,23].
Al-Fe-MgPv (2) = same, TiO_2-free.
Al-Fe-MgPv (3) = peridotite-related Al-Fe-Mg-perovskite [24].

periclase and perovskite, based on the ruby scale [25], and Al_2O_3 solubility in $MgSiO_3$-perovskite [26]. The pressure uncertainty was determined to be 0.5 GPa; the temperature uncertainty was estimated to be 30°C.

2.2. Analytical techniques

Mineral compositions were measured by the electron microprobe (JEOL Superprob, JXA-8800M) under operating conditions of 15 kV and 10 nA specimen current. The phases were also identified by the micro-area X-ray powder diffractometer (MacScience M18XCE) and micro-Raman spectrometer (Jasco NRS-2000). An Ar^+ laser with a wavelength of 514.5 nm and a laser power of 12 mW was focused to a sample area of about 1 μm in diameter.

Water contents were determined by FTIR and SIMS. Infrared spectra were measured using a Jasco MFT-2000 microsampling FTIR spectrometer. Measurements were carried out using a tungsten light source, a Ge-coated KBr beam splitter and a high-sensitivity, wide-band MCT detector. Several hundred scans were accumulated for each spectrum with 1 cm^{-1} resolution and 50 or 100 μm apertures. During the measurements, the microscope was not purged with a stream of free gas, but the effect of absorbed water on the sample surface was found to be negligible by measurements on samples with different thicknesses. Background corrections of absorbance spectra were carried out by a spline fit of the baseline defined by points outside the OH stretching region. We used unpolarized radiation to measure water contents. Therefore, water contents were obtained by averaging the absorbances measured on several sample sections from the same run.

Micro-FTIR spectra were measured for double-polished thin sections of polycrystalline aggregates or single crystal perovskites placed on a KBr plate. The thicknesses of the thin sections and separate single crystals were varied from 120 to 20 μm, but the majority of them were about 70 μm thick. The concentrations of hydroxyl groups were determined by the method of Paterson [27] where absorption bands were integrated by using the calibration of the extinction coefficient and density factors (Table 2) calculated similarly to those of Bolfan-Casanova et al. [17]:

$$C_{OH} = \frac{X_i}{150\xi}\int\frac{K(\overline{\nu})}{(3780-\overline{\nu})}d\overline{\nu}$$

where C_{OH} is the concentration of hydroxyl (in H/10^6 Si or ppm wt. H_2O), ξ is an orientation factor, which is 1/3 for isotropic minerals, and $K(\overline{\nu})$ is the absorption coefficient in cm^{-1} for a given wavenumber $\overline{\nu}$. X_i is a density factor, of which the values are given in Table 2.

Some samples were studied by SIMS for comparison with the FTIR data. We used the same technique and calibration as that described by Murakami et al. [19]. The spot size of the primary ion beam (10 μm) was smaller than the size of the

Table 2
Density factors X_i for different perovskites

Mineral	Sample	X_1 [a] (ppm H_2O)	X_2 [b] (H/10^6 Si)
$MgSiO_3$-perovskite	K-201	2190	2443×10^4
Al-Fe-Mg-perovskite (MORB)	K-205	1978	2527×10^4
Al-Fe-Mg-perovskite (peridotite)	K-208	2123	2469×10^4

Density factors were calculated as described in Bolfan-Casanova et al. [17].
[a] C (ppm H_2O) = C (mol H/l) $\times X_1$ with $X_1 = 10^6\times(18/2d)$, where d is the mineral density (g/l).
[b] C (H atoms/10^6 Si) = C (mol H/l) $\times X_2$ with $X_2 = 10^6\times(M/d)$, where M is the molar mass (g/mol).

grains (typically 40–120 μm). Accordingly, we could avoid the grain boundary effect.

To determine the $Fe^{3+}/\Sigma Fe$ ratio in three MORB-related perovskites, we performed electron energy loss spectroscopy (EELS) measurements on a transmission electron microscopy (TEM). One sample was prepared under liquid nitrogen cooling by argon ion beam thinning in a Gatan Duomill machine (3 kV, 0.7 mA). The other two samples were simply crushed under liquid nitrogen cooling and then loaded onto holey carbon grids. In both cases, liquid nitrogen was used to avoid amorphization of silicate perovskite. The measurements were then performed with a Gatan PEELS 666 (parallel electron energy loss spectrometer) attached to the Philips CM20 FEG scanning TEM at the Bayerisches Geoinstitut, University of Bayreuth. This system reaches an energy resolution of 0.8 eV, measured as half width of the zero loss peak. Fe L_{23} ELNES (electron energy loss near edge structure) spectra were acquired in diffraction mode with convergence α and collection β semi-angles of $\alpha = 8$ mrad and $\beta = 2.7$ mrad. ELNES spectra were gain-normalized, background-subtracted and deconvoluted using the low-loss spectra. The $Fe^{3+}/\Sigma Fe$ ratio was then finally deduced according to the universal method of van Aken et al. [28]. This method is based on the white line intensities at the Fe L_{23} edges and has been calibrated for several mineral groups with iron in the high-spin state [29].

3. Results

3.1. Phase relations

The results of experiments are summarized in Table 3. Experimental products are usually represented by polycrystalline aggregates of perovskite

Table 3
Experimental results

Run No.	Starting material	Pressure (GPa)	Temperature (°C)	Time (min)	Phase assemblage
K-202	A	25	1300	360	MgPv, fl
K-200	B	25	1400	360	Al-MgPv, Gt, fl
K-201	C	25	1400	360	Al-MgPv, Gt
K-165	D	25	1200	720	Al-MgPv, Gt, NAL, fl
K-164	E	26	1200	900	Al-MgPv, Gt, NAL, fl
K-160	F	26	1000[a]	1200	Al-Fe-MgPv, (Rw), fl
K-161	F	26	1200	900	Al-Fe-MgPv, (Rw), fl
K-205	G	25	1300	180	Al-Fe-MgPv, St, fl
K-208	H	25	1400	360	Al-Fe-MgPv, (Br), St, fl
K-209	H	25	1600	120	Al-Fe-MgPv, (Br), St, fl

Phases: MgPv, Mg-perovskite; Al-MgPv, aluminous Mg-perovskite; Al-Fe-MgPv, Al-Fe-Mg-perovskite; St, stishovite; NAL, Na-Al phase; Gt, majorite garnet; (Rw), ringwoodite and (Br), brucite quench microinclusions (see text); fl, fluid or melt.
[a] This experiment was initially heated at 1200°C for 2 h.

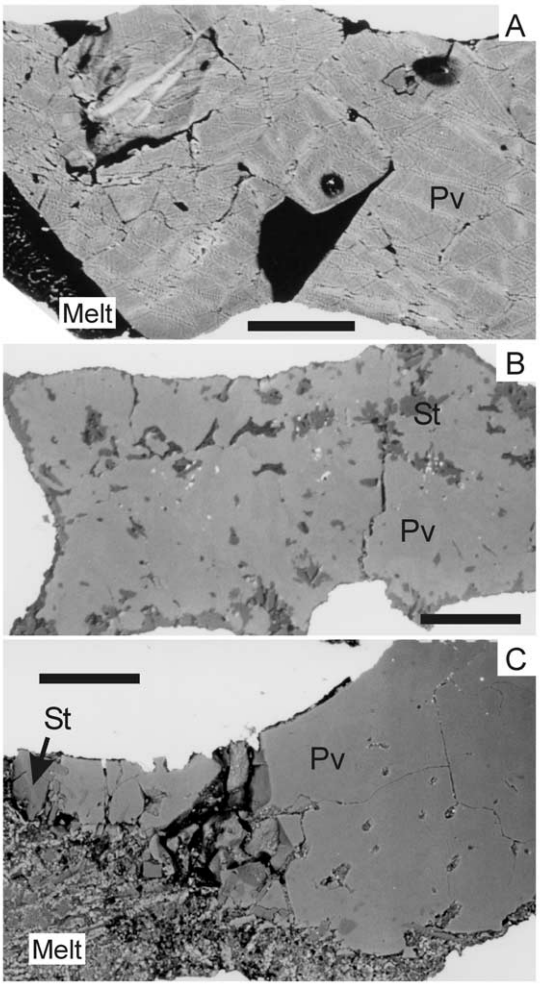

Fig. 1. Back-scattered electron images of experimental products. (A) Sample K-202 (25 GPa, 1300°C), $MgSiO_3$-perovskite. (B) Sample K-205 (25 GPa, 1300°C), Al-Fe-Mg-perovskite related to MORB. (C) Sample K-209 (25 GPa, 1600°C), Al-Fe-Mg-perovskite related to peridotite. Pv, perovskite; St, stishovite. Scale bar correspond to 100 μm.

corresponding to the starting composition with minor amounts of quench crystals of other phases (Fig. 1). Experiments with Mg-rich starting compositions C and D (Table 1) yield phase assemblies of Al-perovskite, majorite garnet, Na-Al phase and fluid. Selected electron microprobe analyses of the perovskites are shown in Table 4. The results indicate normal stoichiometric proportions for $MgSiO_3$- and Al-bearing perovskites. However, for Fe-rich perovskites cation proportions indicate significant amounts of Fe^{3+} incorporated into perovskite.

We measured water contents in four types of Mg-perovskite samples, which can be defined as follows: (1) pure $MgSiO_3$-perovskite; (2) Al-rich Mg-perovskite (denoted as Al-Mg-perovskite; Al_2O_3 = 2–7.2 wt%; Mg# = Mg/(Mg+Fe_{total}) = 100); (3) Mg-perovskite related to MORB (Al-Fe-Mg-perovskite; Al_2O_3 = 13–17 wt%; Mg# = 58–61); and (4) Al-Fe-Mg-perovskite related to peridotite (Al-Fe-Mg-perovskite; Al_2O_3 = 5–6 wt%; Mg# = 88–90).

3.2. *Fe^{3+} in Al-Fe-Mg-perovskite related to MORB*

The measurements of Fe L_{23} ELNES spectra for three MORB-related Al-Fe-Mg-perovskite samples (K-160, K-161, and K-205) consistently show a high content of ferric iron. The Fe L_3 edge is composed of two overlapping white lines at 707.8 and 709.5 eV (Fig. 2), whereby the intensity of the latter peak reflects the ferric iron content. Applying the window method of [28], we found high $Fe^{3+}/\Sigma Fe$ ratios between 0.48 and 0.69, with only one data point below 0.6. The relative errors in these measurements are about 0.05. In recent experimental studies, similarly high ferric iron contents have been detected in anhydrous aluminous silicate perovskite, with the ferric iron positively correlated with the Al

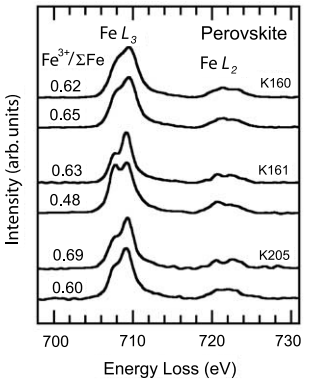

Fig. 2. Fe $L_{2,3}$ edge electron energy loss spectra and $Fe^{3+}/\Sigma Fe$ of MORB-related Al-Fe-Mg-perovskites.

Table 4
Representative perovskite compositions

Sample	K-202 MgPv		K-200a Al-MgPv		K-201 Al-MgPv (dry)		K-165 Al-MgPv		K-164 Al-MgPv		K-160 Al-Fe-MgPv (MORB)		K-161 Al-Fe-MgPv (MORB)		K-205 Al-Fe-MgPv (MORB)		K-208 Al-Fe-MgPv (peridotite)		K-209 Al-Fe-MgPv (peridotite)	
N	4	1σ	4	1σ	4	1σ	6	1σ	5	1σ	8	1σ	6	1σ	7	1σ	8	1σ	11	1σ
SiO_2	60.10	(0.33)	59.09	(0.24)	59.19	(0.05)	57.86	(0.37)	55.37	(0.91)	36.73	(0.82)	38.11	(0.32)	38.43	(0.82)	52.77	(0.82)	53.11	(0.43)
TiO_2											2.18	(0.30)	1.91	(0.08)						
Al_2O_3			2.03	(0.13)	1.45	(0.23)	4.43	(0.35)	7.16	(0.41)	14.50	(0.49)	13.16	(0.25)	16.77	(0.65)	5.50	(0.50)	5.80	(0.43)
FeO*											26.23	(0.92)	24.52	(0.21)	23.40	(1.19)	7.39	(0.49)	6.09	(0.91)
MgO	40.36	(0.21)	39.77	(0.13)	39.78	(0.09)	39.55	(0.18)	38.14	(0.42)	20.15	(0.56)	21.37	(0.21)	20.82	(0.89)	34.48	(0.59)	34.94	(0.37)
H_2O*	0.01		0.01				0.11		0.14		0.01		0.01		0.01		0.18		0.15	
Total	100.47	(0.54)	100.90	(0.26)	100.42	(0.34)	101.95	(0.34)	100.81	(0.94)	99.81	(0.56)	99.08	(0.48)	99.43	(0.26)	100.32	(0.69)	100.09	(0.51)
Si	1.000		0.979		0.985		0.948		0.918		0.683		0.709		0.706		0.903		0.907	
Ti											0.031		0.027							
Al			0.039		0.028		0.086		0.140		0.319		0.289		0.364		0.111		0.117	
Fe^{3+}											0.245		0.229		0.216		0.063		0.052	
Fe^{2+}											0.163		0.153		0.144		0.042		0.035	
Mg	1.000		0.982		0.987		0.966		0.942		0.559		0.593		0.570		0.880		0.889	
Total	2.000		2.000		2.000		2.000		2.000		2.000		2.000		2.000		2.000		2.000	
H	0.001		0.001				0.012		0.015		0.001		0.001		0.001		0.021		0.017	
$2V_O$			0.003		0.002		0.018		0.025		0.008		0.010		0.008		0.019		0.017	
Mg#											57.8		60.8		61.3		89.3		91.1	
$(Mg+Fe^{2+})/(Si+Ti)$	1.000		1.003		1.002		1.019		1.027		1.011		1.013		1.011		1.021		1.019	
Volume (cm^3)	24.43		24.43*		24.43*		24.43*		24.43*		25.33		25.33		25.27		24.69		24.69	
Density (g/cm^3)	4.11		4.11		4.11		4.11		4.12		4.60		4.56		4.51		4.22		4.20	

Volumes were measured by microfocused X-ray diffractometer by measuring the lattice parameters. *Volume for Al-perovskite was assumed to be the same as that in pure $MgSiO_3$-perovskite (K-202). The values of volumes and densities are at 300 K and 1 atm. Values in parentheses represent one standard deviation (1σ). *N*, number of analyses. FeO*, total Fe as FeO. Mg# = 100 Mg/(Mg+Fe_{total}). H_2O*, suggested H_2O content from Table 5. Fe^{3+} was calculated from $Fe^{3+}/\Sigma Fe$ ratio by EELS. $2V_O = (1-Si-Ti)-(1-Mg-Fe^{2+}) = M_B^{3+}-M_A^{3+}$, is amount of oxygen vacancies created by Eq. 1, see text for further explanations. Total EPMA analyses of perovskites are available in Table 6[1].

[1] See online version of this paper.

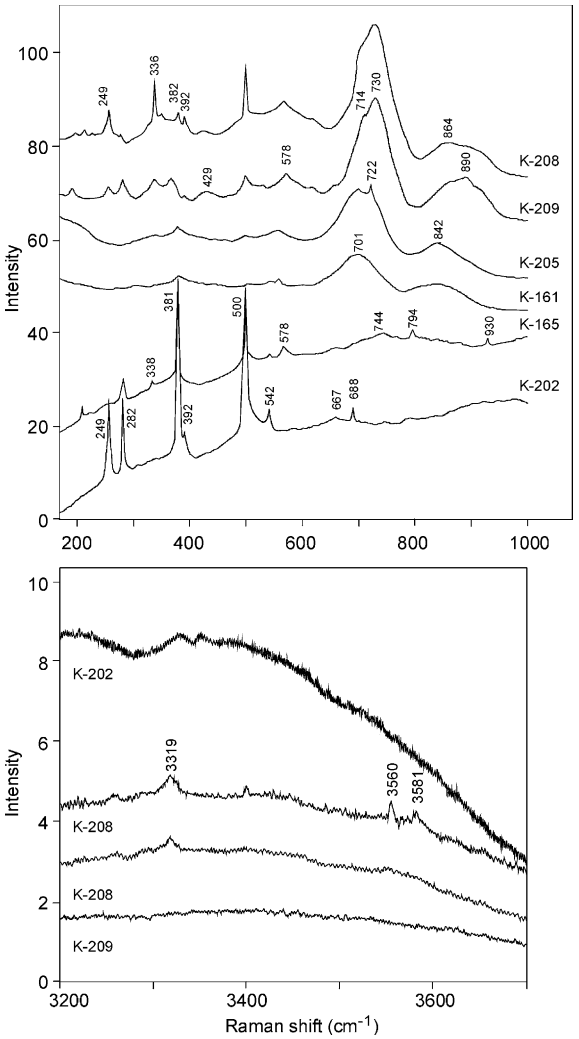

Fig. 3. Raman spectra of different magnesium silicate perovskites. Intensity is given in arbitrary units.

content [30,31]. However, Al-free perovskite contains distinctly less ferric iron [31].

3.3. Raman spectra of perovskites

The Raman spectra of different Mg-perovskites are shown in Fig. 3. The spectrum of $MgSiO_3$-perovskite has major bands at 249, 282, 381, and 500 cm^{-1}. This is consistent with previous data [32,33]. The spectra of Al-Mg-perovskites are generally identical to that of $MgSiO_3$-perovskite, except for the appearance of minor bands at 338, 578, and 930 cm^{-1}. The spectra of Al-Fe-Mg-perovskites from peridotite and MORB samples are similar and differ from the spectra of $MgSiO_3$-perovskite by the presence of two broad bands at 700–730 and 842–890 cm^{-1} (Fig. 3, top). The positions of these bands are, however, different for two types of Al-Fe-Mg-perovskites. MORB-related perovskites have a broad double band with maximum intensities at 701 and 722 cm^{-1} and a band at 842 cm^{-1}, whereas peridotite-related perovskites have a double band at 714 and 730 cm^{-1} and a band at 864–890 cm^{-1}. The broadness of the bands at high frequency may be related to partial amorphization of perovskite formed by thermal decomposition at low pressure [34], or to the character of vibrations of Al atoms in the perovskite structure, because these bands are characteristic for Al-rich phases, NAL and CF (our unpublished data).

We collected several high-quality Raman spectra in the hydroxyl vibration region. The spectra were nearly flat for most samples, except peridotite-related perovskite K-208 (Fig. 3, bottom). Several weak peaks were detected at 3319, 3560, and 3581 cm^{-1}; however, only peaks at 3319 cm^{-1} were reproduced in the second measurement. The peak positioned at 3319 cm^{-1} is close to the band reflecting the major OH vibration in hydrous wadsleyite (3322 cm^{-1}) [33]. These data indicate that water solubility in K-208 may be significant, because the Raman bands related to hydroxyl vibration are generally only visible in case of high OH concentrations.

3.4. Hydroxyl in $MgSiO_3$-perovskite

Unpolarized IR spectra of pure $MgSiO_3$-perovskite synthesized at 25 GPa and 1300°C are shown in Fig. 4. The sample contains clear single crystals free of any optically visible fluid or mineral inclusions. The size of the crystals was close to 100 μm. IR spectra show several bands: one major at 3448 cm^{-1} and three minor at 3397, 3423, and 3482 cm^{-1}. Some minor bands are also identified in the region at 3200–3280 cm^{-1}. The bands at 3423 and 3482 cm^{-1} are consistent with data reported by Meade et al. [16] for $MgSiO_3$-perovskite synthesized at 27 GPa and 1830°C.

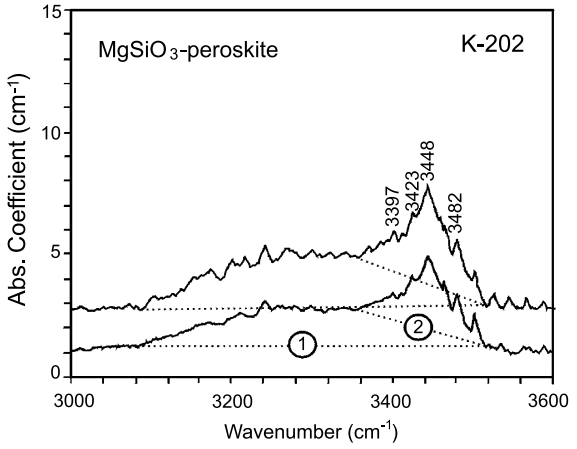

Fig. 4. Examples of unpolarized FTIR spectra of $MgSiO_3$-perovskite synthesized at 25 GPa and 1300°C.

The calculated water content corresponds to about 100 ppm H_2O dissolved in $MgSiO_3$-perovskite (Table 5). This value was calculated using integrated area 1 in Fig. 4. Calculation of water content using integrated area 2 (Fig. 4), ignoring the minor bands at lower wave numbers, suggests near 40 ppm H_2O.

SIMS measurements indicate about 0.03 wt% (300 ppm) H_2O in $MgSiO_3$-perovskite. Although this value is close to the detection limit, the steady-state intensity of hydrogen ions was systematically above the background level in all SIMS measurements. The absence of micrometer-size fluid inclusions was confirmed by monitoring the profile of the hydrogen intensity with sputter time.

This result is different from that obtained by Bolfan-Casanova et al. [17,18] for $MgSiO_3$-perovskite synthesized at 24 GPa and 1600°C, where water was not detected. We can only surmise that differences of our and Meade et al. [16] data from those reported by Bolfan-Casanova et al. may be due to a pressure effect on hydrogen incorporation into Mg-perovskite.

3.5. Hydroxyl in aluminous $MgSiO_3$-perovskite

The grain size of Al-bearing Mg-perovskite is small (usually less than 50 μm) in the samples studied. IR spectra of Al-Mg-perovskite containing 2 wt% Al_2O_3 synthesized at 25 GPa and 1400°C (sample K-200) show a broad band near 3400 cm^{-1}. Minor bands at 3215, 3423, and 3448 cm^{-1} are also observed. The spectra are different from those of anhydrous perovskite (K-201) and indicate water content near 100 ppm (Fig. 5). Although we observed microinclusions in grain boundary regions of the crystals, such a low water content indicates that the microinclusions are not fluid but crystalline inclusions.

Al-Mg-perovskite containing 4–7 wt% Al_2O_3 (K-164 and K-165) shows broad IR spectra with poorly identified bands at 3404, 3448, and 3565 cm^{-1} (Fig. 5). The broadness of the FTIR spectra might be explained by contamination from microinclusions observed around the grain boundaries. The band at 3404 cm^{-1} coincides with the major OH stretching band of superhydrous phase B [35]. Presence of microinclusions of superhydrous

Table 5
Water contents in perovskites measured by FTIR and SIMS

Sample	Temperature (°C)	Mineral	FTIR (ppm H_2O)	1σ	SIMS (wt% H_2O)	1σ
K-202	1300	$MgSiO_3$-perovskite	104	(14)	0.03	(0.01)
K-200	1400	Al-Mg-perovskite (2% Al_2O_3)	101	(19)	–	
K-165	1200	Al-Mg-perovskite (4.5% Al_2O_3)	1101	(156)	0.14	(0.04)
K-164	1200	Al-Mg-perovskite (7.2% Al_2O_3)	1440	(160)	0.14	(0.04)
K-160	1000	Al-Fe-Mg-perovskite (MORB)	110	(21)	0.00	
K-161	1200	Al-Fe-Mg-perovskite (MORB)	104	(26)	0.06	(0.02)
K-205	1300	Al-Fe-Mg-perovskite (MORB)	47	(12)	–	
K-208	1400	Al-Fe-Mg-perovskite (peridotite)	1780	(175)	–	
K-209	1600	Al-Fe-Mg-perovskite (peridotite)	1460	(130)	–	

FTIR H_2O contents were calculated using calibration of Patterson [29] and density factors from Table 2.
Errors were determined by standard deviations of water contents among different crystals in the same sample.

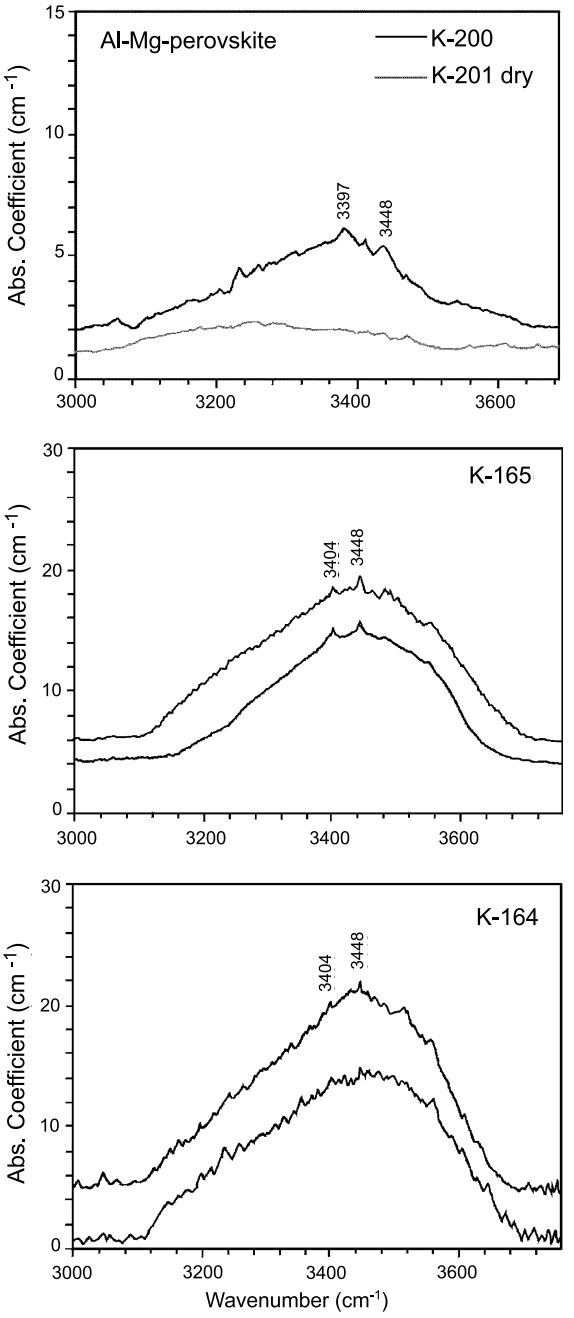

Fig. 5. Examples of unpolarized FTIR spectra of hydrous and dry aluminous $MgSiO_3$-perovskites synthesized at 25 GPa.

phase B may be consistent with MgO-rich starting compositions of the samples K-164 and K-165. However, we should note that the second band of superhydrous phase B located at 3348 cm^{-1} is absent. Monitoring the profile of the hydrogen intensity with sputter time of the SIMS also suggests absence of inclusions of fluid and/or hydrous phases. Therefore, we can address the band at 3404 cm^{-1} to perovskite. Calculated water contents of single crystalline perovskite in samples K-164 and K-165 are 1100–1400 ppm. The data are consistent with SIMS measurements (Table 5).

Comparison of Al_2O_3 contents in anhydrous and hydrous samples, K-201 and K-200, indicates that water can increase the Al_2O_3 solubility in Mg-perovskite as was predicted by Navrotsky [36]. Moreover, the Al_2O_3 content in Mg-perovskite increases with increasing water content in the system; perovskite contains 7.2 wt% Al_2O_3 (K-164) in the system with 10 wt% H_2O, whereas it contains 4.5 wt% Al_2O_3 (K-165), in the system with 5 wt% H_2O (Table 4).

3.6. *Hydroxyl in Al-Fe-Mg-perovskite related to MORB*

The crystals of Al-Fe-bearing Mg-perovskite related to MORB have grain sizes of 50–70 μm. The crystals are translucent under the microscope, but contain a subordinate amount of inclusions. The rims of the crystals are milky, therefore they might contain microinclusions.

The unpolarized spectra of MORB-related Al-Fe-Mg-perovskite are shown in Fig. 6. The spectra are composed of two major bands at 3125 and 3397 cm^{-1} and some minor bands. The minor bands at 3423 and 3448 cm^{-1} are consistent with $MgSiO_3$- and Al-bearing Mg-perovskite. The other minor bands, which can be observed in most spectra, are located at ~3250, ~3280 and ~3320 cm^{-1}. These minor bands along with possible impurities can cause a broadening of the spectra. The position of the major band at 3397 cm^{-1} remains constant and is different from the major band of superhydrous phase B (3350 and 3404–3409 cm^{-1}) coexisting with perovskite in the experiments by Bolfan-Casanova [18].

The nature of the band at 3125 cm^{-1} is not

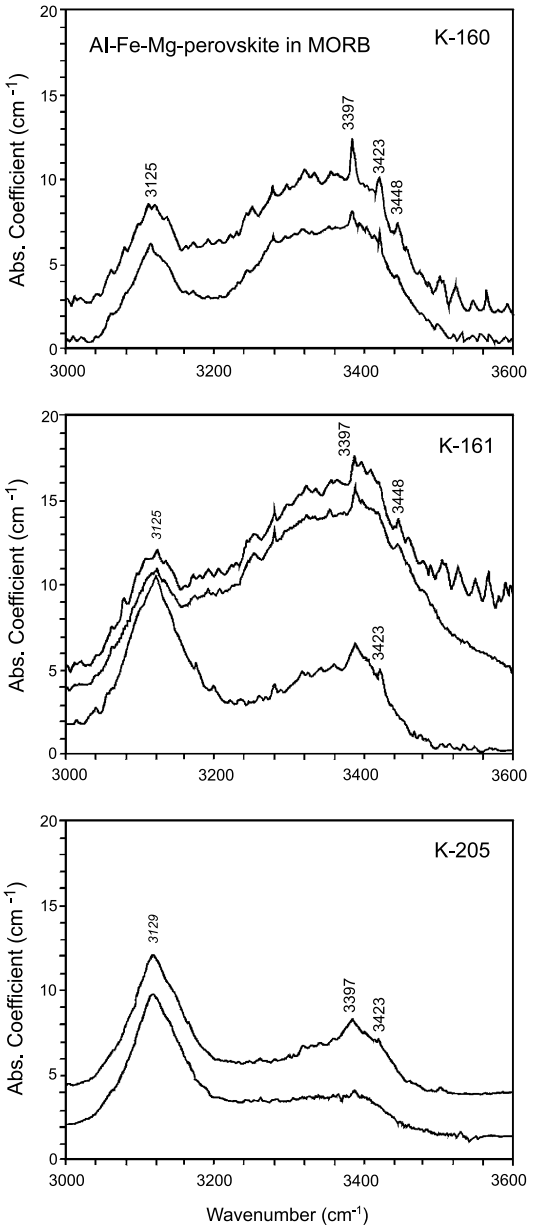

Fig. 6. Examples of unpolarized FTIR spectra of MORB-related Al-Fe-Mg-perovskite synthesized at 25–26 GPa and 1000–1200°C.

clear. It locates away from the majority of bands related to OH vibration in perovskite. This band is close to the major band of ringwoodite at 3120 cm^{-1} [9,17] and stishovite at 3111 cm^{-1} [37]. Even though ringwoodite was not detected by X-ray diffraction and EPMA measurements, we have no other explanation than to address this band to ringwoodite. Possible existence of stishovite inclusions can be ruled out, because the intensity of the OH vibration band in stishovite is very low. Therefore, stishovite inclusions cannot produce a band with intensity comparable to that of the major perovskite band at 3397 cm^{-1} (Fig. 6).

The water content in MORB-related Al-Fe-Mg-perovskites measured by the band at 3397 cm^{-1} is 40–110 ppm. There is a small temperature dependence of water solubility in MORB-related perovskite. The sample synthesized at 1300°C contains less water than those synthesized at 1200 and 1000°C.

3.7. *Hydroxyl in Al-Fe-Mg-perovskite related to peridotite*

The crystals of Al-Fe-bearing Mg-perovskite related to peridotite have grain sizes of 70–80 μm in sample K-208 and >100 μm in sample K-209 (Fig. 1). Similar to MORB-related perovskite the rims of the crystals are milky and may contain microinclusions.

The unpolarized spectra of peridotite-related Al-Fe-Mg-perovskite synthesized at 25 GPa and 1400–1600°C are shown in Fig. 7. The spectra of thick (80–120 μm) samples are broad and are composed of two major bands at 3397 and 3690 cm^{-1}. However, in thin samples other bands at 3215, 3448, 3482, and 3565 cm^{-1} are observed. In the thinnest crystals the intensity of the band at 3215 cm^{-1} is comparable to that of the major band at 3397 cm^{-1}. The position of the major perovskite band at 3397 cm^{-1} is close to that determined by Bolfan-Casanova [18] at 3388 cm^{-1}.

The band at 3690 cm^{-1} is absent in the spectra of thin crystals and may correspond to quench inclusions of brucite (which has a major band at 3698 cm^{-1}) as suggested by Bolfan-Casanova et al. [18]. The band at 3690 cm^{-1} was not used in the calculations of H_2O contents. The H_2O content in Mg-perovskite related to peridotite calculated for samples with an average thickness of 70–80 μm is 1400–1800 ppm. The water content in samples synthesized at 1400°C is slightly higher

than those in samples synthesized at 1600°C. The results are consistent with data of Murakami et al. [19].

4. Discussion

4.1. Comparison with previous studies

The relatively broad absorption spectra indicate not only possible contamination by fluid and mineral inclusions but also complex speciation of water in perovskite. This is partially supported by several minor peaks, which were identified in the OH stretching region in Al-Fe-Mg-perovskite (Figs. 6 and 7). The inclusions are not visible under the microscope, but they obviously exist in thick sample sections in which we identified absorption bands of ringwoodite (MORB-related perovskites), brucite (peridotite-related perovskites), and possibly superhydrous phase B (Al-bearing perovskite). Such small inclusions might have been formed by exsolution from perovskite during quenching. It is not possible, however, to completely avoid the influence of the inclusions close to grain boundaries. They may affect the H_2O content measured by FTIR since spectra show broadening of bands and an increase of the background. To minimize this problem, we selected the sharpest spectra of the sample with sufficient thickness for the calculation of the water content.

SIMS studies indicate that Al- or Al-Fe-bearing Mg-perovskite can accommodate significant amounts of H_2O. Murakami et al. [19] reported 0.1–0.4 wt% H_2O in Al-Fe-Mg-perovskite synthesized from hydrous peridotite KLB-1 at 25.5 GPa. Sanehira et al. [38] reported 0.3–0.4 wt% H_2O in Al-bearing Mg-perovskite synthesized at 27 GPa. Higo et al. [39] also reported 0.05 wt% H_2O in pure $MgSiO_3$-perovskite measured by SIMS in a sample synthesized at 22 GPa. Measurements of H_2O in perovskite by FTIR show systematically lower concentrations. The present results and data by Murakami et al. [19] suggest that Al-bearing Mg-perovskite and Al-Fe-Mg-perovskite related to peridotite can contain thousands of ppm H_2O.

Bolfan-Casanova [18] reported broad IR spectra with a maximum intensity near 3400 cm^{-1} similar to those in Figs. 6 and 7 for Al-Fe-Mg-perovskite containing microinclusions. In contrast, IR spectra of clear perovskite by Bolfan-Casanova [18] have no bands in the OH vibration region. There are some important differences between the present work and the study by Bolfan-Casanova [18]: (1) our Al-Fe-Mg-perovskites (related to peridotite) contain more Al_2O_3 and Fe_2O_3 (+FeO), which should increase the water solubility; (2) we detected several minor peaks, which may affect broadening of the spectra; (3) the location of the major band at 3397 cm^{-1}

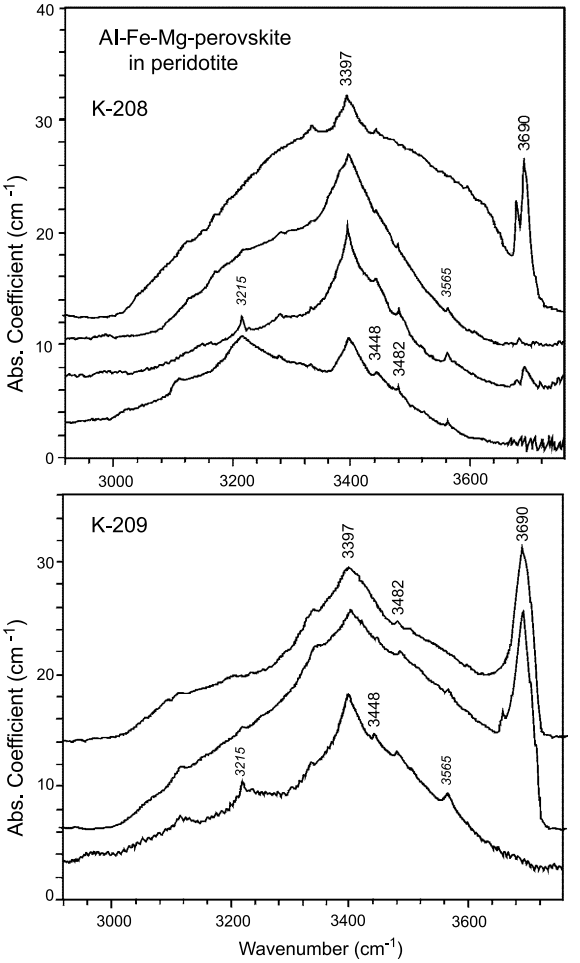

Fig. 7. Examples of unpolarized FTIR spectra of peridotite-related Al-Fe-Mg-perovskite synthesized at 25 GPa and 1400–1600°C. Two lower spectra for sample K-208 were collected from single crystals of 20–30 μm thick.

is very stable; (4) minor peaks were detected in the hydroxyl vibration region by Raman spectroscopy.

Despite these differences we can conclude from the above-mentioned data that Al-Fe-Mg-perovskite related to natural fertile peridotite can accommodate significant amounts of water (up to 0.2 wt% H_2O). Aluminous Mg-perovskites contain up to about 0.15 wt% H_2O if the Al_2O_3 content is 4.5–7.2 wt%. Water solubilities in pure $MgSiO_3$-perovskite and Al-Fe-Mg-perovskite related to MORB are restricted to about 0.01 wt% H_2O.

4.2. *Substitution mechanism of water in the perovskite structure*

Substitution of Al or Fe^{3+} for Si in perovskite can create oxygen defects, which potentially absorb hydrogen. Water solubility in Al-Mg-perovskite increases with increasing Al_2O_3 content. The restricted water solubility in Al- and Fe-rich perovskite related to MORB (with highest Al_2O_3 and FeO_{total} contents) may disagree with this suggestion and requires additional explanation. The EELS spectra of Al-Fe-Mg-perovskite related to MORB indicate that it contains a large amount of ferric iron, $Fe^{3+}/\Sigma Fe \approx 0.6$. This ratio is similar to those reported for peridotite-related perovskites [31,40]; however, the total amount of Fe^{3+} in perovskite is much higher. We suggest that the incorporation of Fe^{3+} into the perovskite structure may have a significant influence on the water solubility.

The potential water solubility in Mg-perovskite was discussed by Navrotsky [36], applying data on ceramic perovskites, which can readily absorb water, to natural systems. According to [36], the defect equilibria in natural perovskites are dominated by the following substitutions in $A^{2+}B^{4+}O_3$:

$$2Si_B^{4+} = 2M_B^{3+} + V_O \quad (1)$$

$$V_O + O_O^{2-} + H_2O = 2OH_O^- \quad (2)$$

where subscripts O and B denote oxygen and B-cation sites, respectively and $M^{3+} = Al^{3+}$ or Fe^{3+}. Eq. 1 creates oxygen vacancies, V_O, and Eq. 2 fills them. Alternatively, the incorporation of trivalent cations such as Al and Fe into $MgSiO_3$-perovskite can follow a coupled substitution of two trivalent cations for silicon and magnesium according to [41]:

$$Mg_A^{2+} + Si_B^{4+} = M_A^{3+} + M_B^{3+} \quad (3)$$

Fe^{3+} has a larger ionic radius than Al^{3+}, which is closer to the ionic radius of Si^{4+} in the B site. Therefore, it is reasonable to suggest that Si^{4+} substitution and oxygen vacancy formation (Eq. 1) is the favorable mechanism in case of Al^{3+}, whereas the coupled substitution on B and A sites (Eq. 3) by two trivalent ions is favored for Fe^{3+}. Atomistic simulations at low pressure confirm this suggestion [42]; however, extrapolation to pressures above 30 GPa implies that vacancy-free substitution may become favorable for Al also, because the volume increases upon vacancy formation. It was suggested that Eq. 3 should be the dominant defect formation mechanism in mantle perovskites [36], in agreement with experimental study [31]. Recently, Frost and Langenhorst [31] have shown that the substitution mechanism in silicate perovskite also changes with Al concentration. At low Al concentrations oxygen vacancies are produced (Eq. 1) but at higher Al concentration, the Al^{3+} moves preferentially on the B sites, whereas Fe^{3+} balances it on the A site (Eq. 3). As a consequence we have fewer vacancies in Fe^{3+}-rich systems and therefore less hydrogen solubility.

These considerations ignore the fact that perovskite coexists with other minerals, like magnesiowüstite and stishovite, which can buffer the defect equilibria in perovskite. Navrotsky [36] argued that excess of MgO in the system can support oxygen vacancy substitution. This is consistent with our experimental results. Al-Mg-perovskite (samples K-164, K-165) synthesized from MgO-rich starting materials (Table 1, D and E) contains a significant amount of water compared to those from MgO-poor starting materials. In addition, MORB-related perovskite synthesized from MgO-poor starting material contains very low H_2O contents compared to peridotite-related perovskite synthesized from MgO-rich starting material.

There is no structural site for water incorporation in pure $MgSiO_3$-perovskite. However, hydrogen can be incorporated into Mg-perovskite as hydroxyl point defects as was proposed for nominally anhydrous minerals like olivine and pyroxene [7–10].

Although some uncertainties are expected from the stoichiometric calculation of electron microprobe analyses we can calculate the amount of oxygen vacancies and therefore potential water solubility in perovskite by oxygen vacancy substitution (Table 4, Fig. 8). The oxygen vacancies (V_O) created by the mechanism of Eq. 1 can be calculated as $2V_O = (1-\text{Si-Ti})-(1-\text{Mg-Fe2+}) = M_B^{3+}-M_A^{3+}$ if we assume that equal amounts of trivalent cations (Al^{3+} and Fe^{3+}) in site B and in site A were involved in the substitution according to Eq. 3. These vacancies can be replaced by OH^- groups according to Eq. 2. For simplicity, $2V_O$ is denoted as the amount of oxygen vacancies below in the text, which should correspond to the amount of hydrogen in the perovskite formula.

From these calculations we can conclude that 30 and 35% of the Al^{3+} in site B (samples K-165 and K-164, respectively) create oxygen vacancies in Al-Mg-perovskite according to Eq. 1, whereas the other 65–70% of Al^{3+} in site B are charge-balanced according to Eq. 3. Calculated contents of oxygen vacancies in Al-Mg-perovskite of K-165 and K-164 are 0.018 and 0.025 atoms per formula unit (a.p.f.u.). Most of these vacancies are occupied by hydrogen as shown in Table 4.

The cation values of peridotite perovskite (samples K-208 and K-209 in Table 4) indicate that 12–20% of the M^{3+} cations in site B create 0.012–0.017 a.p.f.u. oxygen vacancies according to Eq. 1. However, in MORB-related perovskite only 2–4% of trivalent cations in site B create oxygen vacancies by Eq. 1 (samples K-160, K-161, K-205 in Table 4). The high Fe^{3+} content in MORB-related perovskite suggests that trivalent cations favor substitution of Mg and Si sites by the mechanism of Eq. 3 (Fig. 8), consistently with data by Frost and Langenhorst [31]. This explains restricted water solubility in MORB perovskites, which contain less than 0.010 a.p.f.u. of oxygen vacancies (Table 4).

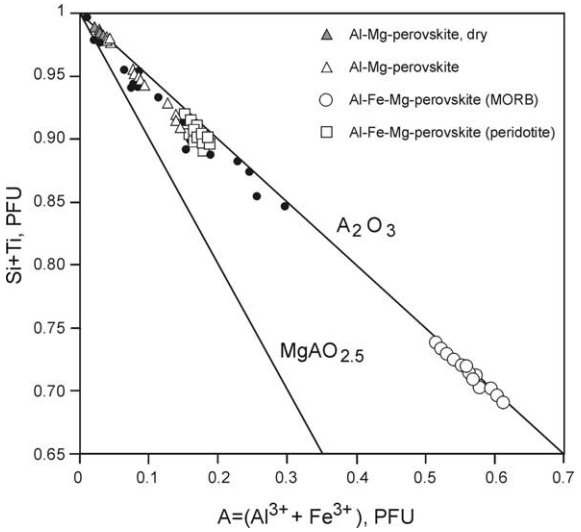

Fig. 8. The variation of Si+Ti content of perovskite with combined trivalent atoms ($A^{3+} = Al^{3+}+Fe^{3+}$). Two curves for substitution mechanism by Eq. 1 $MgAO_{2.5}$ and Eq. 3 A_2O_3 are indicated. Filled circles, data from [30,31].

4.3. Water storage capacity of the lower mantle

There are three sources of water in the Earth's lower mantle: (1) primordial water stored in the early Earth evolution; (2) water transported from the ocean by descending slabs; (3) water expelled from a hydrogen-saturated outer core [2,3]. At least the second source is obvious because water can be transported by dense hydrous magnesium silicates like superhydrous phase B and phase G/D. The stability fields of these phases are limited to the uppermost lower mantle [43,44]. Therefore, this region can be considered to be important as the dehydration region of the lower mantle.

The significant water solubility in peridotite-related Al-Fe-Mg-perovskite suggests that the lower mantle can store a considerable amount of water. Average fertile lower mantle peridotite consists of 80 wt% Mg-perovskite, 15 wt% magnesiowüstite, and 5 wt% Ca-perovskite (e.g. [45,46]). Ca-perovskite and magnesiowüstite can accommodate about 0.3–0.4 and 0.2 wt% H_2O respectively [19], but these data contradict results reported in [47,48]. Taking into account that the water content in the phases decreases with increasing temperature (up to the mantle geotherm), we can es-

timate that the average lower mantle peridotite can contain 0.15 wt% H_2O. Therefore, the maximum amount of water in the lower mantle is estimated as 3.42×10^{21} kg. This is 2.5 times the present ocean mass and comparable with the amount of water potentially stored in the transition zone.

Comparison of hydrous pyrolite and hydrous MORB indicates that pyrolite is a more efficient water carrier in the mantle. Pyrolite includes dense hydrous magnesium silicates, existing under the conditions of subducting slabs. At the normal mantle and hotter conditions pyrolite contains hydrous wadsleyite or ringwoodite in the transition zone and water-bearing Mg-perovskite (+Ca-perovskite and magnesiowüstite) [19] in the lower mantle. In the MORB composition, lawsonite and phengite are stable up to 12–13 GPa under the slab conditions [5,49]. At higher pressures and temperatures, the distribution of water to the MORB perovskite and other phases is very restricted [20].

Acknowledgements

We are grateful to H. Keppler, A. Navrotsky and two anonymous reviewers for very constructive comments during the review process. The authors are thankful to Y. Ito for assistance with the EPMA measurement and N. Miyajima for help during TEM preparation. K.L. thanks the Center for Northeast Asian Studies of Tohoku University and Japanese Society for the Promotion of Science for research fellowships. This work was supported by a Grant-in-Aid of Scientific Research of the Ministry of Education, Science, Sport, and Culture of the Japanese government to E.O. and to H.Y.*[BW]*

References

[1] A.E. Ringwood, Composition of the core and implications for origin of the earth, Geochem. J. 11 (1977) 111–135.
[2] T. Okuchi, Hydrogen partitioning into molten iron at high pressure: Implications for Earth's core, Science 278 (1997) 1781–1784.
[3] Q. Williams, R.J. Hemley, Hydrogen in the deep Earth, Annu. Rev. Earth Planet. Sci. 29 (2001) 365–418.
[4] A.B. Thompson, Water in the Earth's mantle, Nature 358 (1992) 295–302.
[5] B.O. Mysen, P. Ulmer, J. Konzett, M.W. Schmidt, The upper mantle near convergent plate boundaries, in: R.J. Hemley (Ed.), Ultrahigh-Pressure Mineralogy, Physics and Chemistry of the Earth's Deep Interior, Rev. Mineral. 37 (1998) 97–138.
[6] D.J. Frost, The stability of dense hydrous magnesium silicates in Earth's transition zone and lower mantle, in: Y. Fei, C.M. Bertka, B.O. Mysen (Eds.), Mantle Petrology: Field Observations and High Pressure Experimentation: A Tribute to F.R. Boyd, Geochem. Soc. Spec. Publ. 6 (1999) 283–296.
[7] D.R. Bell, G.R. Rossman, Water in Earth's mantle: the role of nominally anhydrous minerals, Science 255 (1992) 1391–1397.
[8] J. Ingrin, H. Skogby, Hydrogen in nominally anhydrous upper-mantle minerals: concentration levels and implications, Eur. J. Mineral. 12 (2000) 543–570.
[9] D.L. Kohlstedt, H. Keppler, D.C. Rubie, Solubility of water in the α, β, and γ phases of $(Mg,Fe)_2SiO_4$, Contrib. Mineral. Petrol. 123 (1996) 345–357.
[10] M. Kurosawa, H. Yurimoto, S. Sueno, Patterns in the hydrogen and trace element compositions of mantle olivines, Phys. Chem. Miner. 24 (1997) 385–395.
[11] T. Inoue, H. Yurimoto, Y. Kudoh, Hydrous modified spinel, $Mg_{1.75}SiH_{0.5}O_4$: a new water reservoir in the mantle transition region, Geophys. Res. Lett. 22 (1995) 117–120.
[12] E. Ohtani, H. Mizobata, H. Yurimoto, Stability of dense hydrous magnesium silicate phases in the system Mg_2SiO_4-H_2O and $MgSiO_3$-H_2O at pressures up to 27 GPa, Phys. Chem. Miner. 27 (2000) 533–544.
[13] M.W. Schmidt, L.W. Finger, R.J. Angel, R.E. Dinnbier, Synthesis, crystal structure, and phase relations of $AlSiO_3OH$, a high-pressure hydrous phase, Am. Mineral. 83 (1998) 881–888.
[14] E. Ohtani, T. Shibata, T. Kubo, T. Kato, Stability of hydrous phases in the transitional zone and the upper most part of the lower mantle, Geophys. Res. Lett. 22 (1995) 2552–2556.
[15] D.J. Frost, Y. Fei, Stability of phase D at high pressure and high temperature, J. Geophys. Res. 103 (1998) 7463–7474.
[16] C. Meade, J.A. Reffner, E. Ito, Synchrotron infrared absorbance measurements of hydrogen in $MgSiO_3$ perovskite, Science 264 (1994) 1558–1560.
[17] N. Bolfan-Casanova, H. Keppler, D. Rubie, Water partitioning between nominally anhydrous minerals in the MgO-SiO_2-H_2O system up to 24 GPa: implications for the distribution of water in the Earth's mantle, Earth Planet. Sci. Lett. 182 (2000) 209–221.
[18] N. Bolfan-Casanova, The Distribution of Water in the Earth's Mantle: An Experimental and Infrared Spectroscopic Study, PhD Thesis, Universität Bayreuth, 2000.

[19] M. Murakami, K. Hirose, H. Yurimoto, S. Nakashima, N. Takafuji, Water in Earth's lower mantle, Science 295 (2002) 1885–1887.
[20] K. Litasov, E. Ohtani, H. Yurimoto, The influence of water on phase transitions and melting temperature of basalt at high pressure: implication for mantle plume, Abstracts of the Superplume International Workshop, Tokyo Institute of Technology, 2002, pp. 380–381.
[21] K. Hirose, Y. Fei, Y. Ma, H.-K. Mao, The fate of the subducted basaltic crust in the Earth's lower mantle, Nature 397 (1999) 53–56.
[22] K. Hirose, Y. Fei, Subsolidus and melting phase relations of basaltic composition in the uppermost lower mantle, Geochim. Cosmochim. Acta 66 (2002) 2099–2108.
[23] K. Litasov, E. Ohtani, Phase relations and melt compositions in CMAS-pyrolite-H_2O system up to 25 GPa, Phys. Earth Planet. Inter. 134 (2002) 105–127.
[24] A. Suzuki, E. Ohtani, H. Morishima, T. Kubo, T. Okada, H. Terasaki, T. Kato, T. Kikegawa, In situ determination of the phase boundary between wadsleyite and ringwoodite in Mg_2SiO_4, Geophys. Res. Lett. 27 (2000) 803–806.
[25] L. Chudinovskih, R. Boehler, High-pressure polymorphs of olivine and the 660-km seismic discontinuity, Nature 411 (2001) 574–577.
[26] A. Kubo, M. Akaogi, Post-spinel transitions in the system Mg_2SiO_4-$Mg_3Al_2Si_3O_{12}$ up to 28 GPa: phase relations of garnet, ilmenite and perovskite, Phys. Earth Planet. Inter. 121 (2000) 85–102.
[27] M.S. Paterson, The determination of hydroxyl by infrared absorption in quartz, silicate glasses and similar materials, Bull. Mineral. 105 (1982) 20–29.
[28] P.A. van Aken, B. Liebscher, V.S. Styrsa, Quantitative determination of iron oxidation states in minerals using Fe $L_{2,3}$-edge electron energy-loss near-edge structure spectroscopy, Phys. Chem. Miner. 5 (1998) 323–327.
[29] P.A. van Aken, B. Liebscher, Quantification of ferrous/ferric ratios in minerals: new evaluation schemes of Fe L_{23} electron energy-loss near-edge spectra, Phys. Chem. Miner. 29 (2002) 188–200.
[30] S. Lauterbach, C.A. McCammon, P. van Aken, F. Langenhorst, F. Seifert, Mössbauer and ELNES spectroscopy of (Mg,Fe)(Si,Al)O_3 perovskite: a highly oxidized component of the lower mantle, Contrib. Mineral. Petrol. 138 (2000) 17–26.
[31] D. Frost, F. Langenhorst, The effect of Al_2O_3 on Fe-Mg partitioning between magnesiowüstite and magnesium silicate perovskite, Earth Planet. Sci. Lett. 199 (2002) 227–241.
[32] D.J. Durben, G.H. Wolf, High-temperature behavior of metastable $MgSiO_3$ perovskite: a raman spectroscopic study, Am. Mineral. 77 (1992) 890–893.
[33] P.F. McMillan, R.J. Hemley, P. Gillett, Vibrational spectroscopy of mantle minerals, in: M.D. Dyar, C. McCammon, M.W. Schaefer (Eds.), Mineral Spectroscopy: A Tribute to Roger G. Burns, Geochem. Soc. Spec. Publ. 5 (1996) 175–213.
[34] R.J. Hemley, R.E. Cohen, A. Yeganen-Haeri, H.-K. Mao, D.J. Weidner, E. Ito, Raman spectroscopy and lattice dynamics of $MgSiO_3$-perovskite at high pressure, in: A. Navrotsky, D. Weidner (Eds.), Perovskite: A Structure of Great Interest to Geophysics and Material Sciences, AGU Geophys. Monogr. 45 (1989) 35–44.
[35] H. Cynn, A.M. Hofmeister, P.C. Burnley, A. Navrotsky, Thermodynamic properties and hydrogen speciation from vibrational spectra of dense hydrous magnesium silicates, Phys. Chem. Miner. 23 (1996) 361–376.
[36] A. Navrotsky, Mantle geochemistry: A lesson from ceramics, Science 284 (1999) 1788.
[37] A. Pawley, P.F. McMillan, J.R. Holloway, Hydrogen in stishovite, with implications for mantle water content, Science 261 (1993) 1024–1026.
[38] T. Sanehira, T. Irifune, T. Inoue, N. Nishiyama, Synthesis of hydrous aluminous perovskite (in Japanese), Abstracts of the 43th High Pressure Conference, Japan, Rev. High Pressure Sci. Technol. 12 (2002) 208.
[39] Y. Higo, T. Inoue, T. Irifune, H. Yurimoto, Effect of water on the spinel-postspinel transformation in Mg_2SiO_4, Geophys. Res. Lett. 28 (2001) 3505–3508.
[40] C. McCammon, Perovskite as a possible sink for ferric iron in the lower mantle, Nature 387 (1997) 694–696.
[41] L.M. Hirsch, T.J. Shankland, Point defects in (Mg,Fe)SiO_3 perovskite, Geophys. Res. Lett. 18 (1991) 1305–1308.
[42] N.C. Richmond, J.P. Brodholt, Calculated role of aluminium in incorporation of ferric iron into magnesium silicate perovskite, Am. Mineral. 83 (1998) 947–951.
[43] S.R. Shieh, H.-K. Mao, R.J. Hemley, L.Ch. Ming, Decomposition of phase D in lower mantle and the fate of dense hydrous silicates in subducting slabs, Earth Planet. Sci. Lett. 159 (1998) 13–23.
[44] E. Ohtani, M. Toma, K. Litasov, T. Kubo, A. Suzuki, Stability of hydrous phases and water storage capacity in the transitional zone and lower mantle, Phys. Earth Planet. Inter. 124 (2001) 105–117.
[45] S.E. Kesson, J.D. FitzGerald, J.M. Shelley, Mineralogy and dynamics of a pyrolite lower mantle, Nature 393 (1998) 253–255.
[46] B.J. Wood, Phase transformations and partitioning relations in peridotite under lower mantle conditions, Earth Planet. Sci. Lett. 174 (2000) 341–354.
[47] N. Bolfan-Casanova, S. Mackwell, H. Keppler, C. McCammon, D. Rubie, Pressure dependence of H solubility in magnesiowüstite up to 25 GPa: Implications for the storage of water in the Earth's lower mantle, Geophys. Res. Lett. 29 (2002) 10.1029/2001GL014457.
[48] K. Litasov, E. Ohtani, Effect of Al_2O_3 on water solubility in lower mantle ferropericlase: preliminary results, Abstract volume, Eur. Union Geosci. 12, Geophys. Res. Abst. 5 (2003) 5875.
[49] M.W. Schmidt, S. Poli, Experimentally based water budgets for dehydrating slabs and consequences for arc magma gemeration, Earth Planet. Sci. Lett. 163 (1998) 361–379.